Appendix for:

MICAL2PV suppresses the formation of tunneling nanotubes and modulates mitochondrial trafficking in lung cancer cells

Fei Wang[1,2], Xiaoping Chen[3], Haipeng Cheng[3], Lu Song[1], Jianghong Liu[1], Steve Caplan[4], Li Zhu[1,2,*] and Jane Y. Wu[3,*]

[1]State Key Laboratory of Brain and Cognitive Science, Institute of Biophysics, Chinese Academy of Sciences, Beijing, China; [2]University of Chinese Academy of Sciences, Beijing, China; [3]Department of Neurology, Center for Genetic Medicine, Lurie Cancer Center, Northwestern University Feinberg School of Medicine, Chicago, Illinois, USA; [4]Department of Biochemistry and Molecular Biology, University of Nebraska Medical Center, Omaha, Nebraska, USA.

Table of Contents:

Appendix Figure S1.
Appendix Figure S2.
Appendix Figure S3.
Appendix Figure S4.
Appendix Figure S5.

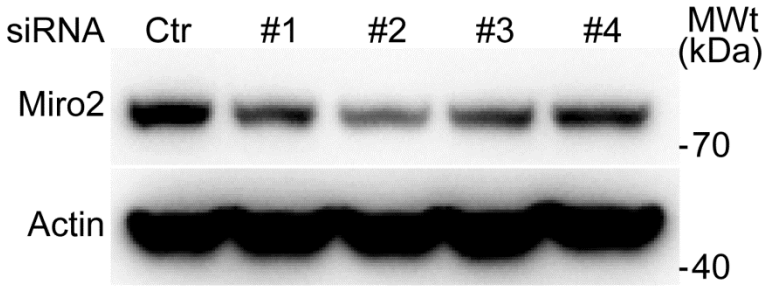

Appendix Figure S1. Efficiency of down-regulating Miro2 expression by different siRNAs.

H1299 cells were transfected with control or different siRNAs against Miro2 (100 pmol). Following transfection, cells were harvested and cell lysates were used in Western blotting using anti-Miro2 antibody. Transfection with #2 Miro2 siRNA significantly reduced the Miro2 protein level; and this siRNA was used in subsequent experiments.

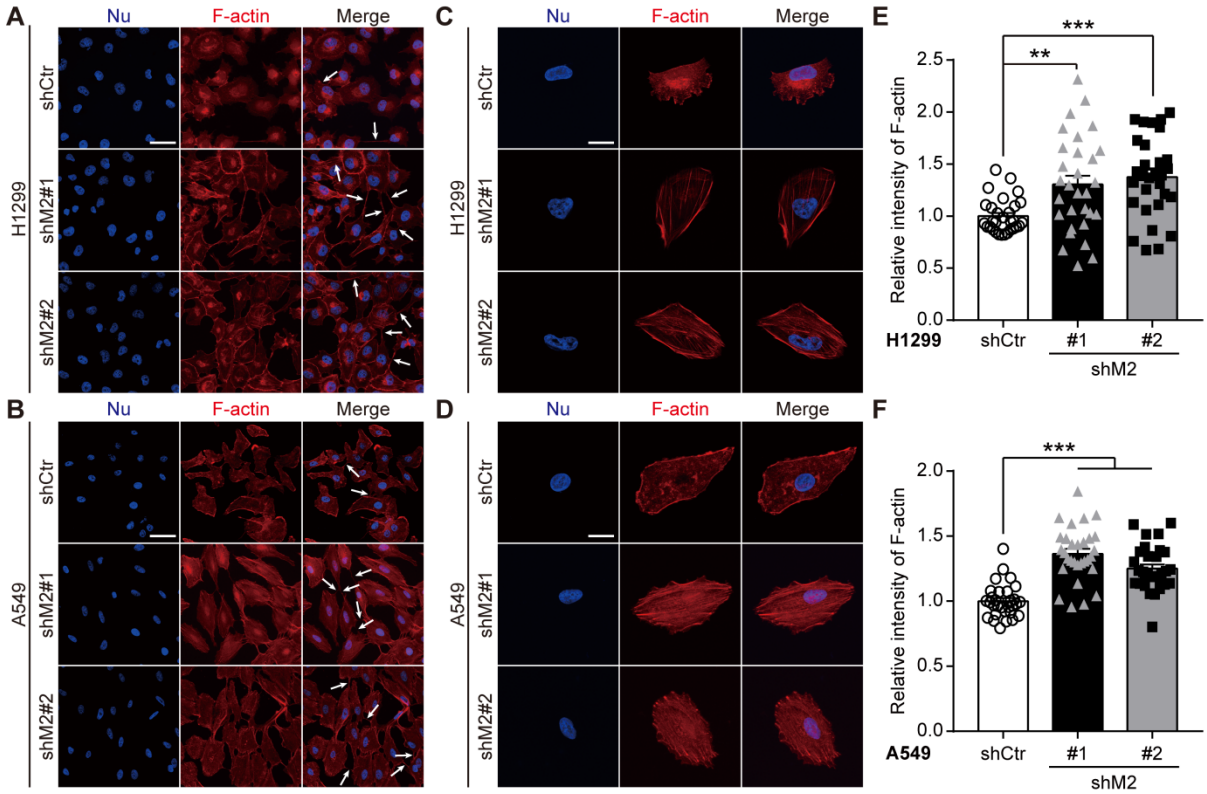

Appendix Figure S2. Down-regulating MICAL2PV promotes F-actin formation.

A, B Control and shM2 H1299 (A) or shM2 A549 (B) cells were stained with phalloidin (red) to detect F-actin. The white arrowheads marked the TNTs. Scale bar: 50 μm

C, D F-action formation was examined at higher magnification in control and shM2 H1299 (C) and A549 (D) cells. Scale bar: 20 μm

E, F Under the same imaging settings, images were taken from each group. To quantify fluorescence signal intensity of F-actin, original non-enhanced images were analyzed using ImageJ and normalized to cells in the control group. 30 images were quantified in three independent experiments.

Data information: In (A-D), nuclei were stained with Hoechst 33342 (blue). Data were analyzed using one-way ANOVA and shown as mean ± SEM; **:$P < 0.01$, ***:$P < 0.001$. In order to visualize the morphological differences and F-actin distribution more clearly, the fluorescence images shown in panels A-D were enhanced in contrast and brightness.

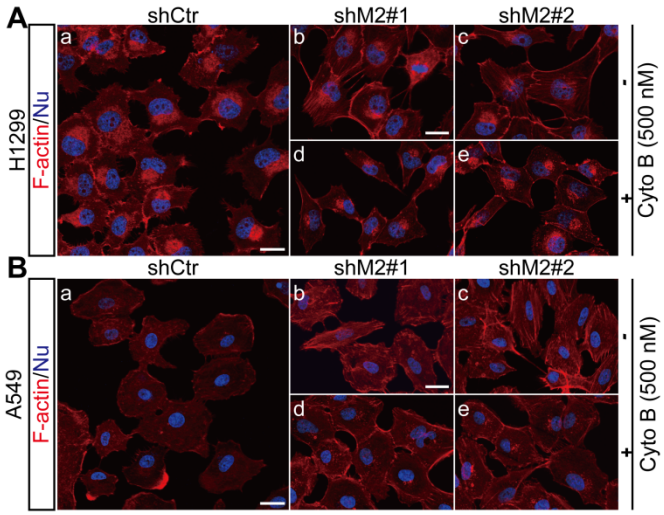

Appendix Figure S3. Cytochalasin B treatment of shM2 cells restores F-actin morphology to that in untreated control cells.

A, B The shM2 H1299 (**A**) and A549 (**B**) cells were treated by 500 nM Cytochalasin B (Cyto B, 500nM) (d, e) or DMSO (b, c) for 24 h followed by confocal microscopy. F-actin morphology was compared with untreated control cells (a) and Cytochalasin B treated shM2 cells (d, e) or with non-treated shM2 cells (b, c). Scale bar: 25 μm.

Data information: In (A, B), nuclei were stained with Hoechst 33342 (blue).

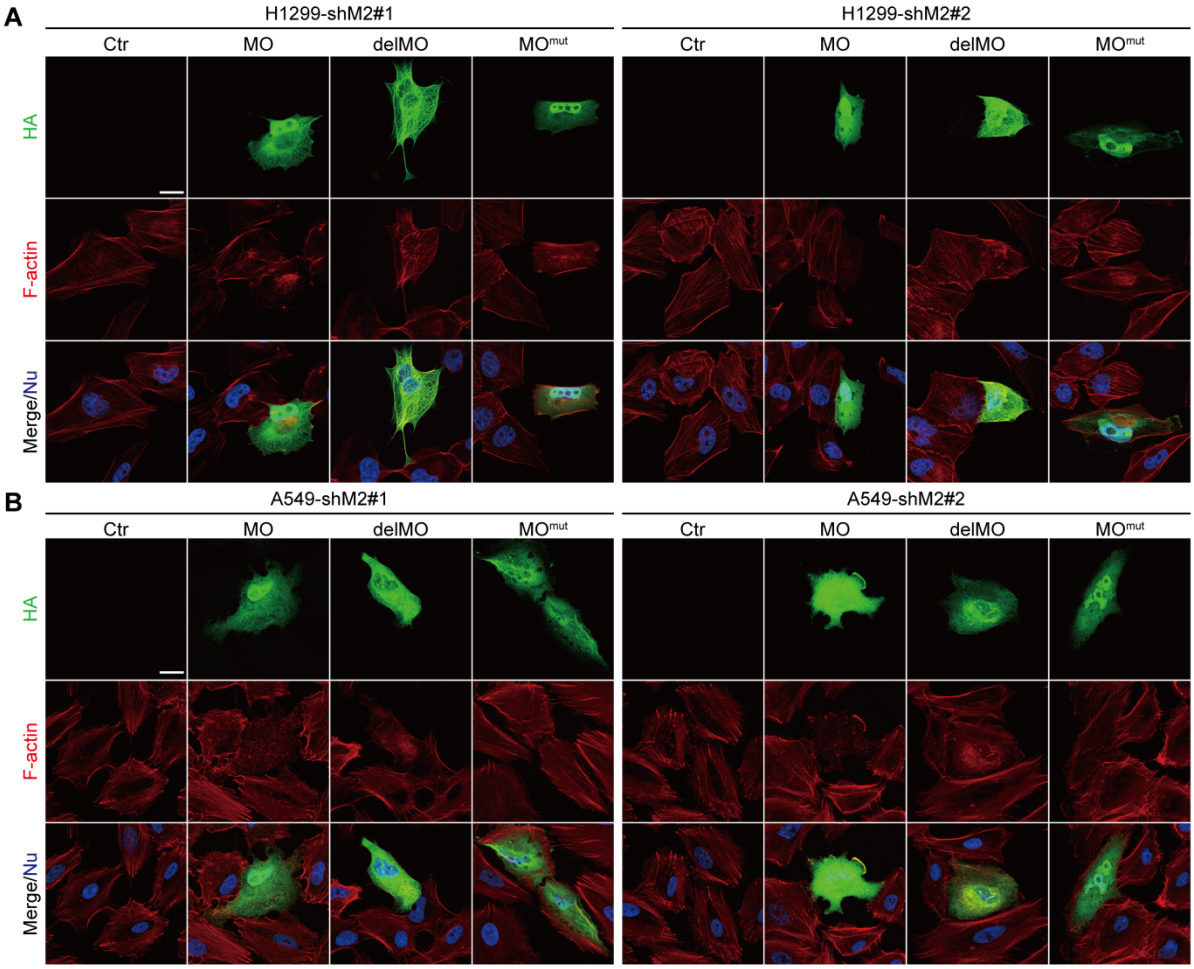

Appendix Figure S4. MICAL2PV mutant lacking the MO domain or with FAD binding site mutated MO domain lost its activity in depolymerizing F-actin.

A, B shM2 H1299 (**A**) and A549 (**B**) cells transfected with different MICAL2PV mutants were stained using phalloidin (red) and anti-HA antibody (green) followed by confocal microscopy. Scale bar: 20 μm.

Data information: In (A, B), nuclei were stained with Hoechst 33342 (blue).

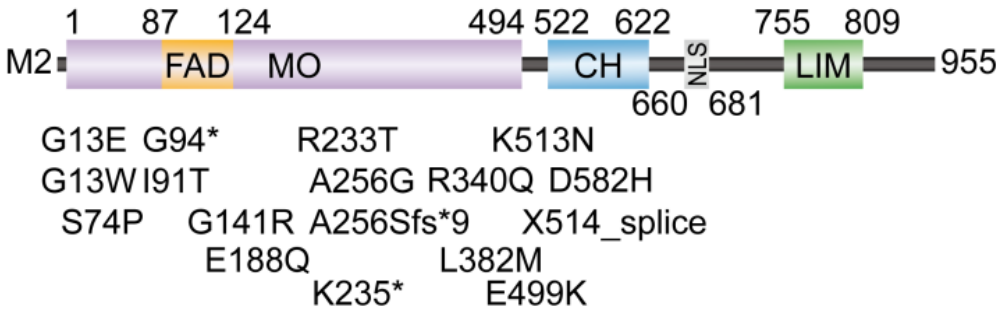

Appendix Figure S5. Domain structure of MICAL2PVb and lung cancer associated mutations in the human MICAL2 gene. Different lung cancer associated mutations identified among lung cancer patients in TCGA dataset are shown. At least 13 mutations have been identified inside the MO domain, with G13 and A256 residues hit by recurrent mutations.